Hindawi
International Journal of Photoenergy
Volume 2018, Article ID 3895013, 11 pages
https://doi.org/10.1155/2018/3895013

Research Article

Performance Optimization of Unglazed Nanofluid Photovoltaic/Thermal System: Energy and Exergy Analyses

M. Imtiaz Hussain[1] **and Jun-Tae Kim**[2]

[1]*Green Energy Technology Research Center, Kongju National University, Cheonan, Republic of Korea*
[2]*Department of Architectural Engineering, Kongju National University, Cheonan, Republic of Korea*

Correspondence should be addressed to Jun-Tae Kim; jtkim@kongju.ac.kr

Received 21 February 2018; Accepted 23 April 2018; Published 3 June 2018

Academic Editor: Kei Ohkubo

The focus of this paper is to predict the transient response of a nanoengineered photovoltaic thermal (PV/T) system in view of energy and exergy analyses. Instead of a circular-shaped receiver, a trapezoidal-shaped receiver is employed to increase heat transfer surface area with photovoltaic (PV) cells for improvement of heat extraction and thus achievement of a higher PV/T system efficiency. The dynamic mathematical model is developed using MATLAB® software by considering real-time heat transfer coefficients. The proposed model is validated with experimental data from a previous study. Negligible discrepancies were found between measured and predicted data. The validated model was further investigated in detail using different nanofluids by dispersing copper oxide (CuO) and aluminum oxide (Al_2O_3) in pure water. The overall performance of the nanoengineered PV/T system was compared to that of a PV/T system using water only, and optimal operating conditions were determined for maximum useful energy and exergy rates. The results indicated that the CuO/water nanofluid has a notable impact on the energy and exergy efficiencies of the PV/T system compared to that of Al_2O_3/water nanofluid and water only cases.

1. Introduction

One of the major challenges facing the world today is the increase in concentrations of greenhouse gases in the environment, which is generally considered as being caused by the substantial use of fossil fuels. Due to the limited availability of fossil fuels and rising air pollution, the replacement of fossil resources by renewable energy has become inevitable. Among various types of renewable energy sources, sun-based energy is the most promising in terms of accessibility, affordability, and cleanliness. The direct conversion of sunlight into electrical energy can be carried out with photovoltaic (PV) cells [1]. Continuous exposure of PV surfaces to the solar radiation in high ambient temperature results in a decrease in device electrical efficiency. Therefore, accumulated solar heat across the PV module is removed through circulation of heat transfer fluids [2, 3]. This integration of a PV module and a thermal collector is called a photovoltaic/thermal (PV/T) system; such a system can viably generate heat and electricity simultaneously.

Over the years, a substantial number of studies have been carried out to find a suitable heat transfer fluid that can effectively extract heat from the PV module. Various heat transfer fluids such as water, glycol, ethylene, and acetone have been tried with the purpose of acquiring high collector efficiency [4, 5], but the low thermal conductivity values of these fluids always remain main hurdles to achieving this goal [6]. To cope with this problem, nanofluid as a heat transfer fluid has been introduced. A colloidal solution (nanofluid) can be obtained by dispersion of nanoparticles in base fluid. Generally, the thermal conductivity and heat transfer coefficient of a nanofluid are higher than those of other available fluids [7]. Therefore, colloidal solutions are expected to improve the overall performance of the PV/T system compared to the case of using water only. Tiwari et al. [8] discussed the effects of volume concentration of Al_2O_3 in the base fluid and variations in the mass flow rate of nanofluid on the performance of a flat plate solar collector. Rejeb et al. [9] presented a combined experimental and numerical study to evaluate the influence of alumina and copper nanoparticles

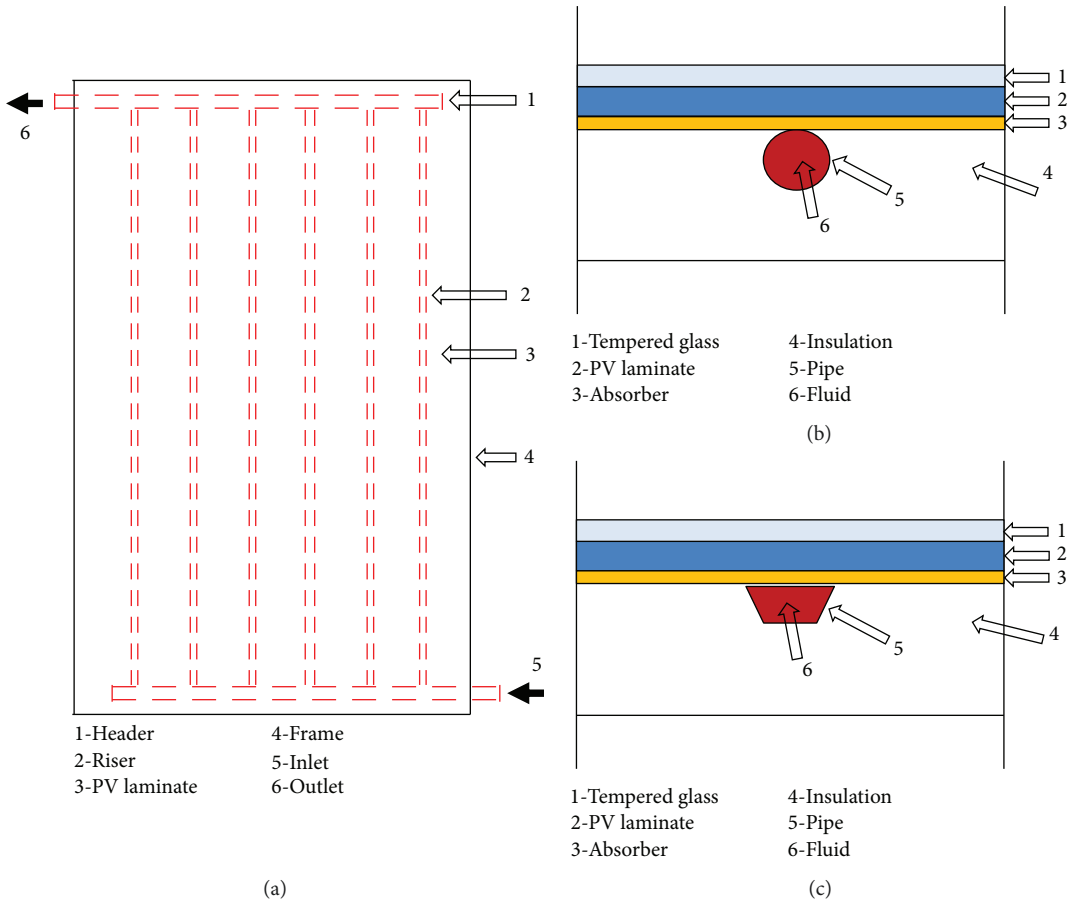

Figure 1: PV/T collector: (a) schematic details, (b) cross section with a circular receiver, and (c) cross section with a trapezoidal receiver.

in different base fluids (water and ethylene glycol) on overall PV/T system performance. It was observed that water as a base fluid gives a higher performance than does ethylene glycol. Hasan et al. [10] proposed a jet impingement cooling system for the PV/T system, in which nozzles directly inject nanofluid (coolant) to the back surface of the PV module. Using jet array nanofluid impingement in the PV/T system, the maximum power of the proposed collector increased by 62.5% in comparison with the conventional PV module. Simultaneous application of nanofluid as a coolant and an organic paraffin wax as a phase change material (PCM) on the exergy and energy efficiencies of the PV/T system is investigated experimentally by Hosseinzadeh et al. [11]. According to the results, the PCM in the nanofluid-based PV/T system immensely enhances the output thermal exergy of the collector. Shahsavar et al. [12] analyzed the exergy performance of a naturally ventilated PV/T air collector in which a thin metal sheet is introduced in the middle of an air passage to improve the heat exchanger performance and thus achieve lower PV temperature.

A considerable number of studies available in the literature indicate that the exergy and energy analyses of the PV/T system have been performed considering steady-state heat transfer conditions. To the best of the authors' knowledge, a few attempts have been made to calculate the comprehensive transient behavior of various PV/T components for the exergy analysis. As pointed out by Jones and Underwood [13], a steady-state model cannot accurately predict the PV temperature responses under rapidly fluctuating solar radiation. To address the aforementioned existing research gaps, a dynamic mathematical model of a PV/T system using nanofluid as a coolant is developed and validated using experimental data from the literature. Interdependence transient processes of the PV/T system were predicted using MATLAB software considering real-time calculation of heat transfer coefficients. To maximize the energy and exergy efficiencies, an optimal mode of operation is determined using different heat transfer fluids and geometrical conditions.

2. Collector Design and Simulation Details

In this study, a sheet and tube PV/T is considered that comprises an off-the-shelf PV module, a thermal absorber, a fluid tube, and thermal insulation. A schematic diagram and a cross-section view of the PV/T system are shown in Figure 1. A monocrystalline silicon cell with ideal conversion efficiency of 15–20% is employed in the PV module. The PV module and the absorber plate are fixed together by means of an adhesive. The fluid carriers (copper tubes) are bonded to the absorber plate at equal spacing in a parallel-flow arrangement throughout the plate width. The absorber plate serves as heat exchanger fins for the fluid tubes. The top and bottom

Table 1: Thermophysical properties of nanoparticles.

Nanoparticles	Properties		
	Specific heat (J/kg·K)	Thermal conductivity (W/m·K)	Density (kg/m^3)
Copper oxide	551	32.9	6310
Aluminum oxide	773	30	3890
Pure water	4179	0.613	997.1

ends of the tubes are connected with common headers to maintain balanced fluid flow and distance between adjacent tubes. The sides and the rear surface of the panel are covered with the thermal insulation to reduce losses due to absorbed solar energy.

Nanoparticles of aluminum oxide (Al_2O_3) and copper oxide (CuO) with a fixed concentration of 0.7 wt% in the base fluid (pure water) were considered in this study. Temperature-dependent thermophysical properties for all utilized heat transfer fluids were determined so that, compared to water as a thermal fluid, the improvements in the heat transfer rate with nanofluid could be evaluated. The properties of the employed heat transfer fluids are shown in Table 1.

Explicit energy flow analysis was performed by modifying the dynamic energy balance equation for the PV/T system given by Chow [14]. The MATLAB ODE solver was used to derive the transient temperatures from the instantaneous energy balance equations. Using the finite difference method [15], a control volume (node) was created, within which the energy and mass balance equations were applied. The parameters considered for the simulation are given in Table 2. Each component of the PV/T system is denoted by node. Therefore, the given collector model consists of a total of five nodes. Figures 1(b) and 1(c) show the temperature nodes for the different PV/T collector components.

3. Mathematical Model

A mathematical model was developed to describe the interdependence of the temperature responses across the different components of the PV/T system. The heat balance across different components of the PV/T system was derived by considering the vicinity of a single copper tube, as all the tubes are arranged in parallel fashion with fixed spacing between them. As indicated by Chow [14], in the parallel-tube arrangement, the temperature and fluid flow rate conditions in all tubes can be assumed to be the same. For the model development, the following assumptions are considered:

(i) The material properties of all components are considered to be constant.

(ii) Considering the same fluid flow rate obtains through all tubes.

(iii) The edge losses are assumed to be negligible.

(iv) The heat transfer coefficients are calculated in real time.

Table 2: Data for simulation.

PV module	Length and width	1.62 m and 0.98 m
	Absorptivity (α_p)	0.9
	Emissivity (ε_p)	0.88
	Specific heat (C_p)	900 J/kg·K
	Packing factor	0.8
	Temperature coefficient (β_r)	0.0045/°C
	Reference PV efficiency (%)	17.3
Copper tube	Inner diameter (D_i)	0.008 m
	Thickness (δ_t)	0.0012 m
	Specific heat (C_t)	903 J/kg·K
	Density (ρ_t)	2702 kg/m^3
	Number of tubes	9
	Tube spacing	0.11 m
Absorber plate	Density (ρ_b)	2702 kg/m^3
	Emissivity (ε_b)	0.87
	Thermal conductivity (K_b)	310 W/m·K
	Thickness (δ_b)	0–1 mm
Insulation	Density (ρ_i)	20 kg/m^3
	Specific heat (C_i)	670 J/kg·K
	Thermal conductivity (K_i)	0.034 W/m·K

3.1. Energy Balance for PV Cells

$$M_p C_p \left(\frac{dT_p}{dt}\right) = G\alpha_p - E - h_{wind}A_{pa}\left(T_p - T_a\right) - h_{ps}A_{ps}\left(T_p - T_s\right) - h_{pb}A_{pb}\left(T_p - T_b\right) - h_{pt}A_{pt}\left(T_p - T_t\right), \quad (1)$$

$$E = GP\eta_{el}, \quad (2)$$

$$\eta_{el} = \eta_r\left[1 - \beta_r\left(T_p - T_r\right)\right], \quad (3)$$

where E is used for electrical power. P is the packing factor and η_e is the electrical efficiency. T_r, η_r, and β_r are the reference PV cell temperature, efficiency, and temperature coefficient, respectively. h_{wind} is the convective heat transfer coefficient due to wind [16]. G and α_p are the solar radiation and absorptivity of the PV cells, respectively; M_p, C_p, and T_p are the mass, specific heat, and temperature of the PV cells, respectively; T_b, T_t, and T_a are the absorber plate, tube, and ambient air temperature, respectively. h_{pa} is the radiative heat transfer coefficient between PV and the sky (T_s). h_{pb} and h_{pt} are the conductive heat transfer coefficients between PV and the absorber and PV and the tube, respectively.

3.2. Energy Balance for Absorber Plate

$$M_b C_b \left(\frac{dT_b}{dt}\right) = h_{pb}A_{pb}\left(T_p - T_b\right) - h_{bt}A_{bt}\left(T_b - T_t\right) - h_{bi}A_{bi}\left(T_p - T_i\right), \quad (4)$$

where T_i is the insulation temperature. M_b and C_b are the

mass and specific heat of the absorber plate, respectively. h_{bt} and h_{bi} are the conductive heat transfer coefficients between the absorber and the tube and the absorber and the insulation, respectively.

3.3. Energy Balance for Tube

$$M_t C_t \left(\frac{dT_t}{dt}\right) = h_{pt}A_{pt}\left(T_p - T_t\right) + h_{bt}A_{bt}(T_b - T_t) - A_{t,fl}h_{t,fl}(T_t - T_{fl}) - A_{ti}h_{ti}(T_t - T_i), \quad (5)$$

where T_{fl} is the circulating fluid temperature. M_t and C_t are the mass and specific heat of the tube, respectively. h_{ti} is the conductive heat transfer coefficient between the tube and the insulation.

3.4. Energy Balance for Insulation

$$M_i C_i \left(\frac{dT_i}{dt}\right) = h_{bi}A_{bi}\left(T_p - T_i\right) - A_{ti}h_{ti}(T_t - T_i) - h_{ia}A_{ia}(T_i - T_a), \quad (6)$$

where M_i and C_i are the mass and specific heat of the insulation material, respectively. h_{ia} is the convective heat transfer coefficient between the insulation and the ambient air.

3.5. Energy Balance for Fluid

$$M_{fl}C_{fl}\left(\frac{dT_{fl}}{dt}\right) = \dot{m}_{fl}C_{fl}\left(T_o - T_{in}\right) + A_{t,fl}h_{t,fl}(T_t - T_{fl}), \quad (7)$$

where $\dot{m}_{fl}$ is the fluid mass flow rate. T_{in} and T_o are the inlet and outlet temperatures of the fluid, respectively. $h_{t,fl}$ is the convective heat transfer coefficient between the tube and the fluid.

3.6. Heat Transfer Coefficients. The convection heat transfer coefficient between PV laminate and ambient air due to wind can be written as

$$h_{wind} = 3u_a + 2.8, \quad (8)$$

where h_{wind} is the convection heat transfer coefficient due to wind and u_a is the wind velocity. The radiation heat transfer coefficient between the PV laminate and the sky is given as follows [17]:

$$h_{ps} = \varepsilon_p \sigma \left(T_p + T_s\right)\left(T_p^2 + T_s^2\right), \quad (9)$$

where ε_p is the emissivity of the PV plate and σ is the Stefan-Boltzman constant. The conduction heat transfer coefficient between the PV laminate and the absorber plate can be calculated using the following equation:

$$h_{pb} = \frac{k_{ad}}{\delta_{ad}}, \quad (10)$$

where k_{ad} and δ_{ad} are the thermal conductivity and thickness, respectively, of the adhesive layer. The conduction heat transfer coefficient between the absorber plate and insulation can be determined as follows [9]:

$$h_{bi} = \frac{2k_i}{\delta_i}, \quad (11)$$

where k_{ad} and δ_{ad} are the thermal conductivity and thickness, respectively, of the insulation. The conductive heat transfer coefficient between the PV laminate and the tube can be expressed using the following correlation [18]:

$$h_{pt}A_{pt} = \frac{\delta_i L}{\left(x_p/2k_p\right) + \left(\delta_{ad}\delta_{ad}/k_{ad}D_o\right)}, \quad (12)$$

$$x_p = \frac{W}{4}, \quad (13)$$

where k_p is the thermal conductivity of the PV plate and W is the tube spacing. D_o and L are the outer diameter and length, respectively, of the tube. The conductive heat transfer coefficient between the absorber plate and the tube can be expressed by the following correlation [14]:

$$h_{bt} = \frac{2k_b}{x_b}, \quad (14)$$

$$x_b = \frac{(W - D_o)}{4}, \quad (15)$$

where k_b is the thermal conductivity of the absorber plate.

The maximum output relative to the ambient temperature can be achieved using exergy analysis. The thermal, electrical, and overall exergy efficiencies given by Yazdanifard et al. [19] for a solar hybrid collector were modified and used for the simulation.

$$\eta_{ex,th} = \frac{\dot{E}_{th}}{\dot{E}_{in}} = \frac{\dot{m}_{fl}C_{fl}(T_o - T_{in})(1 - 293/(293 + (T_o - T_a)))}{\dot{E}_{in}}, \quad (16)$$

$$\eta_{ex,el} = \frac{\dot{E}_{el}}{\dot{E}_{in}} = \frac{GP\eta_r\left[1 - \beta_r\left(T_p - T_r\right)\right]}{\dot{E}_{in}}, \quad (17)$$

$$\eta_{ex,PVT} = \frac{\dot{E}_{th} + \dot{E}_{el}}{\dot{E}_{in}} = \eta_{ex,th} + \eta_{ex,el}, \quad (18)$$

where η_r, T_r, and β_r are the reference efficiency, temperature, and coefficient, respectively; $\eta_{ex,th}$, $\eta_{ex,el}$, and $\eta_{ex,PVT}$ are the thermal, electrical, and overall exergy efficiencies, repectively; $\dot{E}_{th}$ and $\dot{E}_{el}$ are the thermal and electrical exergy rates, respectively. Exergy of the absorbed solar radiation can be calculated using the following expression [19, 20]:

$$\dot{E}_{in} = \left[1 + \frac{1}{3}\left(\frac{T_a}{T_{sun}}\right)^4 - \frac{4T_a}{3T_{sun}}\right]GA_c, \quad (19)$$

where T_{sun} and A_c are the sun temperature and collector area, respectively. The equivalent thermal efficiency can be calculated as

$$\eta_{PVT} = \eta_{th} + \frac{\eta_{el}}{\eta_{pp}}, \quad (20)$$

where η_{PVT}, η_{el}, η_{th}, and η_{pp} are the equivalent thermal efficiency, the electrical and thermal efficiency, and the electrical power generation efficiency of the power plant, respectively. Model calibration for short-term performance evaluation is performed using root mean square error (RMSE) analysis and other statistical indicators, as follows [21, 22]:

$$\mathrm{RMSE}_1 = \left(\frac{1}{n}\sum_{i=1}^{n} d_i^2\right)^{1/2}, \quad (21)$$

$$\mathrm{RMSE}_2 = \left(\frac{1}{n}\sum_{i=1}^{n}\left(\frac{d_i}{Y_i}\right)^2\right)^{1/2}, \quad (22)$$

$$r^2 = \left[\frac{n\left(\sum_{i=1}^{n} X_i Y_i\right) - \left(\sum_{i=1}^{n} X_i\right)\left(\sum_{i=1}^{n} Y_i\right)}{\sqrt{\left[n\sum_{i=1}^{n} X_i^2 - \left(\sum_{i=1}^{n} X_i\right)^2\right]\left[n\sum_{i=1}^{n} Y_i^2 - \left(\sum_{i=1}^{n} Y_i\right)^2\right]}}\right]^2, \quad (23)$$

where d_i is the difference between the ith predicted and measured values, and n is the number of data points. Y_i and X_i are the ith measured and predicted values.

3.7. Model Validation. Authentication of the proposed dynamic model is carried out by comparing predicted results with the published test data of the uncovered PV/T system given by Rejeb et al. [9]. The predicted and measured values of the mean nanofluid temperature were found to be 42.18°C and 41.73°C, respectively. To further determine the reliability, the developed model is validated through comparing the predicted PV cell temperature and the experimental data. The daily PV cell temperature measured by Rommel et al. [23] and predicted results from the mathematical model are presented in Figure 2. For comparison purposes, similar design and operational parameters were considered for each case, as suggested by [9, 23]. It can be seen that the predicted results matched well with the experimental data. There was no apparent deviation or bias between the predicted and the measured results. For model calibration, different statistical indicators were employed [18]. Using RMSE1, RMSE2, and *R*-squared indicators, the obtained values were found to be 0.129, 0.014, and 0.303, respectively. A conclusion can be drawn from the above comparison that the suggested model is reliable at predicting the performance of an unglazed PV/T system even under extreme weather fluctuations.

4. Results and Discussions

It is important to study the influence of nanoparticle concentration on the thermophysical properties, when attempting to evaluate the performance of a nanofluid-based PV/T system. Figure 3 shows the thermal conductivity ratio (k_{nf}/k_{bf}) and

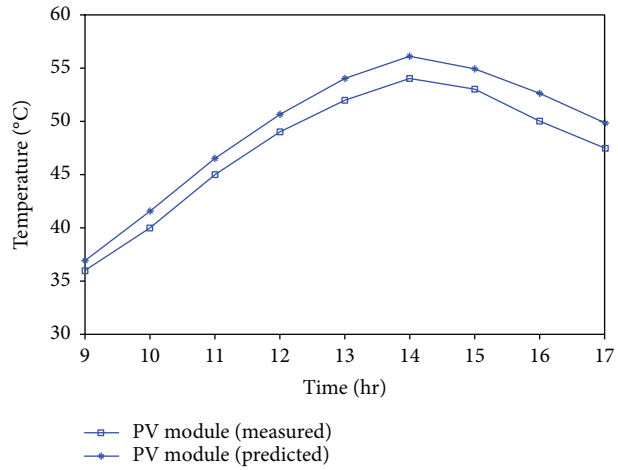

Figure 2: Comparison of measured and predicted PV temperature.

density ratio (ρ_{nf}/ρ_{bf}) enhancement of CuO nanofluid with increasing particle weight fraction. nf and bf stand for nanofluid and base fluid, respectively. The results for Al_2O_3 nanofluid with increasing weight fraction of Al_2O_3 also exhibit a similar trend. However, from the comparison of the thermophysical properties of CuO and Al_2O_3, it is anticipated that a slightly better performance can be obtained when CuO/water is used instead of Al_2O_3/water. On the contrary, an increase in volume fraction of CuO and Al_2O_3 results in a decrease in the marginal specific heat ratio (C_{nf}/C_{bf}) of both nanofluids. The typical value of thermal conductivity for CuO, Al_2O_3, and water are 32.9 W/m·K, 30 W/m·K, and 0.613 W/m·K, respectively. Therefore, colloidal solutions can be anticipated to exhibit notably improved thermophysical properties relative to pure water [24].

The pumping power was calculated from (24) for the trapezoidal and circular receivers and plotted against different concentrations of nanofluids. Figure 4 shows that pressure drop and thus pumping power increase with increasing concentration of the nanofluids. It is observed from the results that pumping powers for both nanofluids are nearly the same. However, CuO nanofluid with a trapezoidal receiver shows the maximum pumping power required than does Al_2O_3 nanofluid with trapezoidal and circular receivers. Compared to other cases considered in this study, the marginally higher pumping power for CuO nanofluid was probably due to the high viscosity [25] and noncircular-shaped of the receive. The pumping power can be expressed as follows:

$$\text{Pumping power} = \left(\frac{\dot{m}_{fl}}{\rho_{fl}}\right) * \Delta p, \quad (24)$$

where ρ_f is the density of circulating fluid, and nanofluid density can be defined as [26]

$$\rho_{nf} = \rho_{np}(\phi) + \rho_{bf}(1-\phi), \quad (25)$$

where ϕ is the concentration of nanoparticles into the base

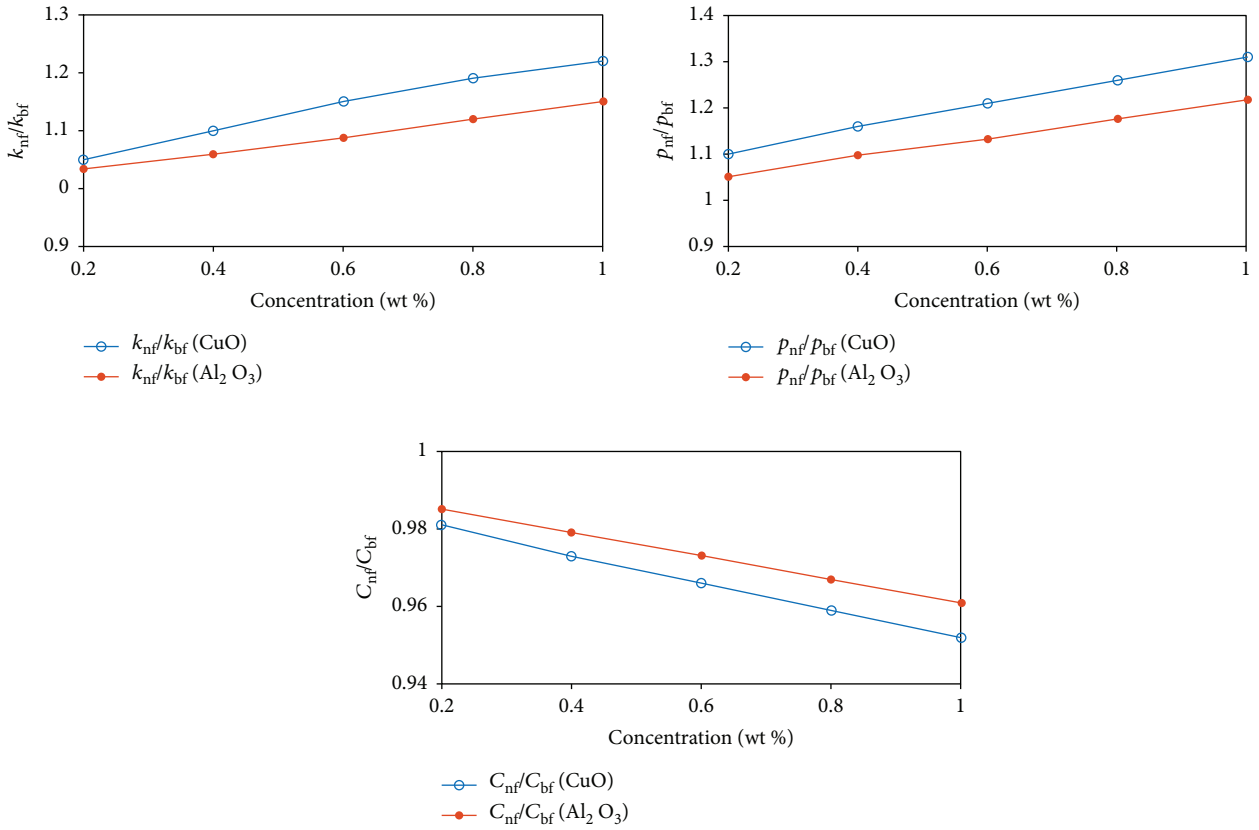

Figure 3: Variations of thermal physical properties of Al_2O_3/water and CuO/water with different concentrations.

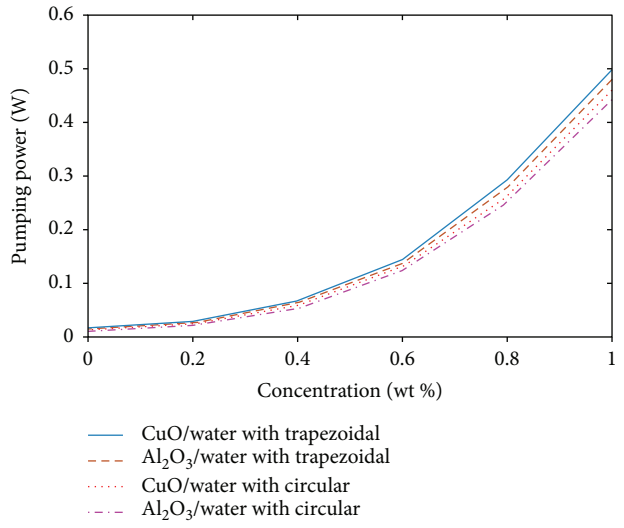

Figure 4: Variation of pumping power with the influence of nanoparticle concentration.

fluid. Pressure drop (Δp) can be calculated using the following correlation [27]:

$$\Delta p = f\frac{\rho_{fl}V^2}{2}\frac{L}{D_i} + K\frac{\rho_{fl}V^2}{2}, \quad (26)$$

where K is the loss coefficient taken according to [27] and V is the fluid velocity in m/s. The friction factor (f) for the laminar and turbulent flow can be expressed as

(1) For laminar flow

$$f = \frac{64}{R_e}. \quad (27)$$

(2) For turbulent flow

$$f = \frac{0.079}{R_e^{0.25}}. \quad (28)$$

R_e is the Reynolds number.

In a tube-and-fin type PV/T collector, the role of the absorber plate, which is sandwiched between the PV module and the fluid pipe, cannot be neglected in the heat transfer process. In fact, variations in the thickness of the absorber plate directly influence the overall performance of the PV/T system. Figure 5 depicts the variations of the thermal and electrical efficiencies of the PV/T system for different thicknesses of the absorber plate. Decreasing the thickness of the absorber plate leads to a decrease in the thermal resistance between the PV module and the circulating fluid. For this reason, the thermal and electrical efficiencies increased. Heat transfer occurs at a faster rate across the thinner absorber plate than it does across the thicker plate. It is worth noting

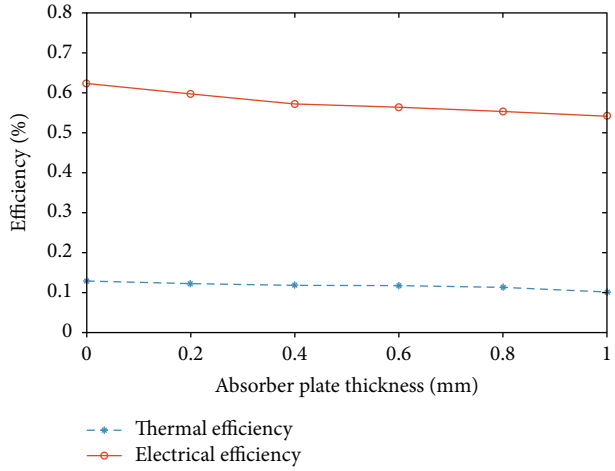

Figure 5: Variations of thermal and electrical efficiency with absorber thickness.

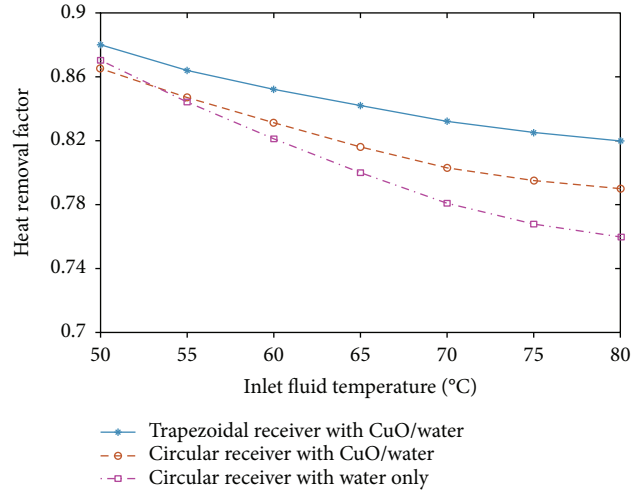

Figure 6: Variations of heat removal factor with inlet fluid temperature using different receiver shapes and fluids.

that the PV/T system without absorber plate (which means zero thickness) shows better overall performance than the PV/T with the absorber plate. Increases of the thermal and electrical efficiency are due to direct contact of the fluid-carrying tubes with the PV rear surface.

Figure 6 shows the relationship between the heat removal factor and the fluid inlet temperature, obtained using different heat transfer fluids and shapes of receivers. For purposes of comparison, the similar surface areas of both the circular- and trapezoidal-shaped receivers were considered. As can be seen, when the inlet fluid temperature increased, the heat removal factors decreased for all cases, independent of the receiver shapes and fluid types. However, the decrease in heat removal factor with the trapezoidal-shaped receiver is much smaller than the decrease when using the circular-shaped receiver. In addition, the trapezoidal receiver with CuO/water as a heat exchanger has a higher heat removal factor than the circular receiver with CuO/water and water. When the inlet fluid temperature increased from 50°C to 80°C, heat removal factors decreased from 0.88 to 0.82, 0.86 to 0.79, and 0.87 to 0.76 for the trapezoidal receiver with nanofluid, circular receiver with nanofluid, and water, respectively. Though the overall heat loss coefficient increased considerably with the fluid temperature, the heat transfer efficiency of the nanofluid did not decrease much because of this material's superior thermophysical properties compared to those of water. This may be attributed to the high thermal conductivity of the nanofluid, even at higher operating temperature. It is also observed that initially at a lower operating temperature the water depicts a marginally higher heat removal factor than nanofluids this was due to low density and the high specific heat of water. As the fluid temperature increases, the density of the nanofluids decreases and contact of nanoparticles with the surface of absorber increases [28], which leads to improvement in heat exchanger performance. Therefore, the heat removal factor for the nanofluid-based PV/T system decreases at a slower rate with increase in inlet fluid temperature.

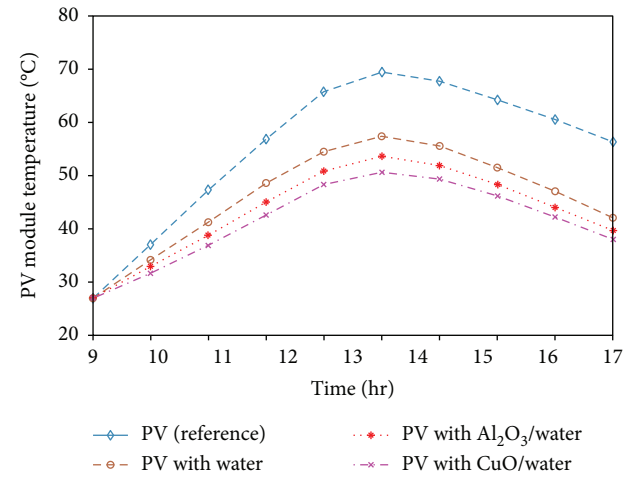

Figure 7: Daily variations of PV temperature with CuO/water, Al_2O_3/water, and water.

The effects of nanofluid as a coolant on the temperature evolution of PV cells are investigated in comparison with the case of pure water. The daily PV cell temperature is evaluated using pure water, Al_2O_3/water, and CuO/water, with results shown in Figure 7. For the purpose of comparative analysis, the PV cell temperature is evaluated with and without coolant fluid. A consensus can be drawn from these results that adding nanoparticles to the water notably reduces the PV cell temperature compared to the sole use of water as the working fluid. Furthermore, the addition of nanoparticles to pure water results in an increase of the overall thermal conductivity of the working fluid and, hence, is the apparent cause of the high outlet fluid temperature. It is noted that the daily maximum reference PV cell temperature obtained without cooling fluid is 69.4°C, while, using water only, Al_2O_3/water, and CuO/water, the values were 57.4°C, 53.7°C, and 50.6°C, respectively. These results show the clear dominance of CuO/water as a heat transfer fluid over Al_2O_3/water in the context of heat removal performance.

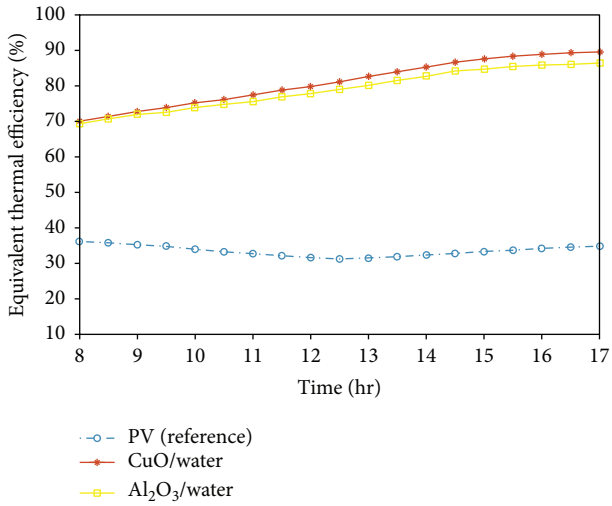

Figure 8: Daily variations of equivalent thermal efficiency with reference PV, CuO/water, and Al_2O_3/water.

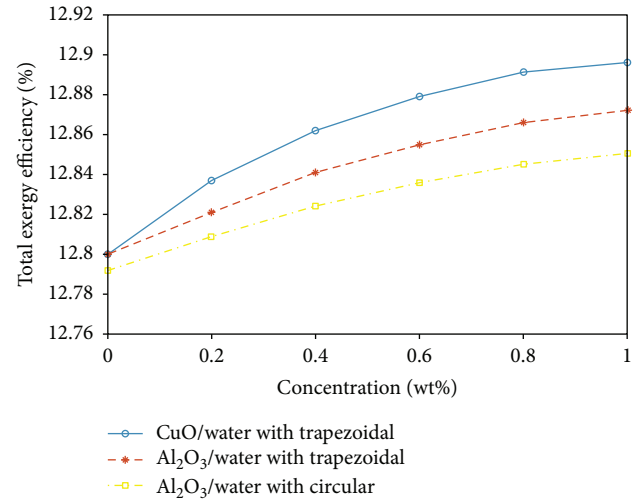

Figure 9: Variations of total exergy efficiency with concentrations (CuO/water and Al_2O_3/water).

Generally, primary energy saving or equivalent thermal efficiency is used as a performance metric for solar hybrid systems. Daily variation of primary energy savings of the PV and the PV/T systems can be obtained by converting electrical energy to equivalent thermal efficiency. Figure 8 shows the daily variation of the equivalent thermal efficiency of the PV and the PV/T systems. The average equivalent thermal efficiency for the PV (reference) is 35.53%; values for the PV/T system with CuO/water and Al_2O_3/water are found to be 80.94 and 78.83%, respectively. In the case of the reference PV cells, the decrease in equivalent thermal efficiency is due to the higher operating temperature that arises from the accumulation of extra solar radiation at the PV surface, in particular during solar noon hours. Primarily, the power output and electrical efficiency of the PV cells are influenced by the operating temperature. It should be noticed that the PV/T system with CuO/water in particular has shown better results than the PV system without coolant and the PV/T system with Al_2O_3/water.

The variation of the exergy efficiency as a function of different concentrations of CuO and Al_2O_3 nanoparticles in the base fluid is presented in Figure 9. Total exergy efficiency values (thermal and electrical) of CuO/water and of Al_2O_3/water were estimated using (18). According to Bejan's narrative [29], the maximum power output is inversely associated with the entropy generation of the solar system. This means that maximization of the power output is equivalent to minimization of the entropy generation rate. It is observed that, independent of nanofluid type, the exergy efficiency of a solar collector increases with increasing nanoparticle concentration in the base fluid. Generally, thermal energy efficiency varies as a function of the outlet temperature and the heat capacity of the thermal fluid. On the other hand, the exergy efficiency is more related to the fluid outlet temperature than to the heat capacity [19]. Therefore, the collector with CuO/water with a trapezoidal receiver showed higher exergy efficiency than did Al_2O_3/water with both trapezoidal- and circular-shaped receivers. This can be explained by the fact that CuO/water as a working fluid offers a higher heat transfer coefficient, which corresponds to a lower PV cell temperature and a higher outlet nanofluid temperature. However, Al_2O_3/water with a trapezoidal receiver performed marginally better than in the case of using Al_2O_3/water with a circular receiver. This is because the direct attachment of a flat top of a trapezoidal receiver onto the PV rear surface increases the total heat transfer surface area and hence improves the heat exchange performance between PV module and the circulating fluid.

Figure 10 shows the total exergy efficiency of the collector as a function of the daily sunlight hours when using Al_2O_3/water, CuO/water, and water as the working fluid. Based on the available solar radiation, the exergetic efficiencies for different working fluids were estimated. It is important to show the relationship between solar radiation and exergy efficiency because irreversibility varies directly with incident solar radiation. It can be clearly seen that the exergy efficiencies when using different fluids follow a pattern similar to the one for daily solar radiation. It is also observed that during the peak sun intensity hours (noon), when the sunlight is strongest, the irreversibility is maximized. Higher solar radiation intensity results in higher temperature difference between the collector surface and the ambient air. A larger difference reflects or may cause extra heat loss from the collector surface and, hence, lowers the exergy efficiency. Therefore, the temperature difference is a key point to consider when attempting to improve exergy efficiency. It is concluded that CuO/water as a heating medium has a profound impact on the collector performance, better than that of Al_2O_3/water and water only.

5. Conclusion

In this study, a transient mathematical model of the nanoengineered PV/T system is proposed based on real-time calculation of all heat transfer coefficients. CuO/water and Al_2O_3/water nanofluids were considered as the heat

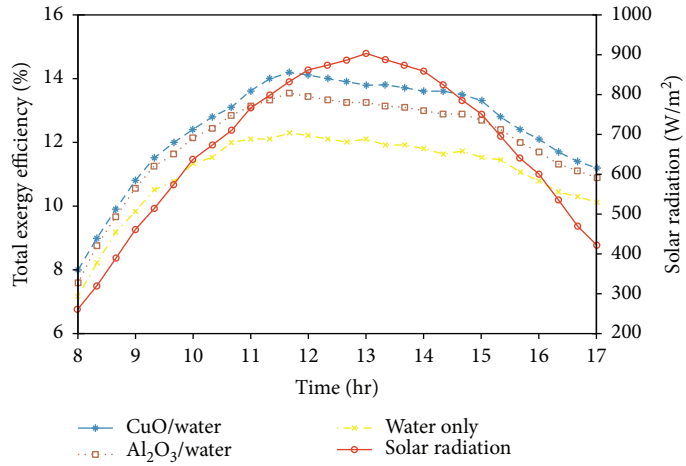

Figure 10: Daily variations of total exergy efficiency with solar radiation (CuO/water and Al_2O_3/water).

transfer fluids. Instead of a circular pipe, a trapezoidal-shaped absorber pipe was used with the intention of improving the surface area and, subsequently, the heat extraction from the PV cells. Experimental validation of the proposed model was performed using outdoor test results from the literature. The optimal energy and exergy efficiencies were located considering different operating conditions. Applying a nanofluid improves the energy and exergy efficiencies of the PV/T system; it was found that the CuO/water nanofluid exhibited better performance than that of the Al_2O_3/water or water-only cases. The highest predicted PV cell temperature without cooling fluid was 69.4°C, whereas, with water, Al_2O_3/water, and CuO/water this value dropped to 57.4°C, 53.7°C, and 50.6°C, respectively. It was observed that the irreversibility of the system increases with increasing solar radiation (at solar noon in particular), which leads to acceleration of heat losses to ambient air and thus results in a considerable exergy loss. The PV/T system with CuO/water nanofluid showed higher exergy efficiency than did the system with Al_2O_3/water nanofluid. The higher exergy efficiency is caused more by the outlet temperature of the CuO/water nanofluid than by the heat capacity.

Nomenclature

M: Mass (kg)
C: Specific heat (J/kg·°C)
T: Temperature (°C)
A: Surface area (m^2)
h: Heat transfer coefficient (W/m^2·°C)
u_a: Wind velocity (m/s)
E: Electrical power (W)
P: Packing factor
G: Solar radiation (W/m^2)
k: Thermal conductivity (W/m·°C)
W: Tube spacing (m)
L: Length (m)
D_i and D_o: Inner and outer tube diameters (m)
$\dot{m}_{fl}$: Mass flow rate (kg/s)
$\dot{E}$: Exergy rate.

Greek

α: Absorptivity
η: Efficiency
η_{PVT}: Primary energy saving efficiency
β_r: Solar cell temperature coefficient (l/K)
ε: Emissivity
σ: Stefan-Boltzmann constant $(W \cdot m^{-2} \cdot K^{-4})$
δ: Thickness (m)
ρ: Density (kg/m^3)
ϕ: Nanoparticle concentration.

Subscripts

p: PV cells
b: Absorber plate
t: Tube
i: Insulation
fl: Circulating fluid
nf: Nanofluid
np: Nanoparticle
bf: Base fluid
a: Ambient air
pp: Power plant
s: Sky
el: Electrical
ex: Exergy
r: Reference
o and in: Outlet and inlet
th: Thermal.

Data Availability

The data used to support the findings of this study are available from the corresponding author upon request.

Conflicts of Interest

The authors declare that there is no conflict of interest regarding the publication of this paper.

Acknowledgments

This work was supported by the Korea Research Fellowship Program through the National Research Foundation of Korea (NRF) funded by the Ministry of Science, ICT, and Future Planning (2016H1D3A1938222); Research Grant from Kongju National University through the Korea Agency for Infrastructure Technology Advancement funded by the Ministry of Land, Infrastructure and Transport of the Korean government (Project no. 17TBIP-C124966-01).

References

[1] J. M. Gordon, "Optimal sizing of stand-alone photovoltaic solar power systems," *Solar Cells*, vol. 20, no. 4, pp. 295–313, 1987.

[2] A. S. Joshi, A. Tiwari, G. N. Tiwari, I. Dincer, and B. V. Reddy, "Performance evaluation of a hybrid photovoltaic thermal (PV/T)(glass-to-glass) system," *International Journal of Thermal Sciences*, vol. 48, no. 1, pp. 154–164, 2009.

[3] M. Imtiaz Hussain, A. Ali, and G. H. Lee, "Multi-module concentrated photovoltaic thermal system feasibility for greenhouse heating: model validation and techno-economic analysis," *Solar Energy*, vol. 135, pp. 719–730, 2016.

[4] S. Chol, *Enhancing Thermal Conductivity of Fluids with Nanoparticles*, vol. 231, ASME-Publications-Fed, 1995.

[5] R. Prasher, P. Bhattacharya, and P. E. Phelan, "Thermal conductivity of nanoscale colloidal solutions (nanofluids)," *Physical Review Letters*, vol. 94, no. 2, 2005.

[6] Z. Said, R. Saidur, M. A. Sabiha, A. Hepbasli, and N. A. Rahim, "Energy and exergy efficiency of a flat plate solar collector using pH treated Al 2 O 3 nanofluid," *Journal of Cleaner Production*, vol. 112, pp. 3915–3926, 2016.

[7] C. H. Li and G. P. Peterson, "Experimental investigation of temperature and volume fraction variations on the effective thermal conductivity of nanoparticle suspensions (nanofluids)," *Journal of Applied Physics*, vol. 99, no. 8, article 084314, 2006.

[8] A. K. Tiwari, P. Ghosh, and J. Sarkar, "Solar water heating using nanofluids–a comprehensive overview and environmental impact analysis," *International Journal of Emerging Technology and Advanced Engineering*, vol. 3, no. 3, pp. 221–224, 2013.

[9] O. Rejeb, M. Sardarabadi, C. Ménézo, M. Passandideh-Fard, M. H. Dhaou, and A. Jemni, "Numerical and model validation of uncovered nanofluid sheet and tube type photovoltaic thermal solar system," *Energy Conversion and Management*, vol. 110, pp. 367–377, 2016.

[10] H. A. Hasan, K. Sopian, A. H. Jaaz, and A. N. al-Shamani, "Experimental investigation of jet array nanofluids impingement in photovoltaic/thermal collector," *Solar Energy*, vol. 144, pp. 321–334, 2017.

[11] M. Hosseinzadeh, M. Sardarabadi, and M. Passandideh-Fard, "Energy and exergy analysis of nanofluid based photovoltaic thermal system integrated with phase change material," *Energy*, vol. 147, pp. 636–647, 2018.

[12] A. Shahsavar, M. Ameri, and M. Gholampour, "Energy and exergy analysis of a photovoltaic-thermal collector with natural air flow," *Journal of Solar Energy Engineering*, vol. 134, no. 1, article 011014, 2012.

[13] A. D. Jones and C. P. Underwood, "A thermal model for photovoltaic systems," *Solar Energy*, vol. 70, no. 4, pp. 349–359, 2001.

[14] T. T. Chow, "Performance analysis of photovoltaic-thermal collector by explicit dynamic model," *Solar Energy*, vol. 75, no. 2, pp. 143–152, 2003.

[15] J. A. Clarke, *Energy Simulation in Building Design*, Routledge, London, 2007.

[16] M. Imtiaz Hussain, G. H. Lee, and J.-T. Kim, "Experimental validation of mathematical models of identical aluminum and stainless steel engineered conical solar collectors," *Renewable Energy*, vol. 112, pp. 44–52, 2017.

[17] M. Imtiaz Hussain and G. H. Lee, "Thermal performance evaluation of a conical solar water heater integrated with a thermal storage system," *Energy Conversion and Management*, vol. 87, pp. 267–273, 2014.

[18] S. Bhattarai, J. H. Oh, S. H. Euh, G. Krishna Kafle, and D. Hyun Kim, "Simulation and model validation of sheet and tube type photovoltaic thermal solar system and conventional solar collecting system in transient states," *Solar Energy Materials and Solar Cells*, vol. 103, pp. 184–193, 2012.

[19] F. Yazdanifard, E. Ebrahimnia-Bajestan, and M. Ameri, "Performance of a parabolic trough concentrating photovoltaic/thermal system: effects of flow regime, design parameters, and using nanofluids," *Energy Conversion and Management*, vol. 148, pp. 1265–1277, 2017.

[20] R. Petela, "Exergy of heat radiation," *Journal of Heat Transfer*, vol. 86, no. 2, p. 187, 1964.

[21] R. J. Stone, "Improved statistical procedure for the evaluation of solar radiation estimation models," *Solar Energy*, vol. 51, no. 4, pp. 289–291, 1993.

[22] D. H. Kim, B. M. Jenkins, T. R. Rumsey, M. W. Yore, and N. J. Kim, "Simulation and model validation of a horizontal shallow basin solar concentrator," *Solar Energy*, vol. 81, no. 4, pp. 463–475, 2007.

[23] M. Rommel, D. Zenhäusern, A. Baggenstos, O. Türk, and S. Brunold, "Development of glazed and unglazed PVT collectors and first results of their application in different projects," *Energy Procedia*, vol. 70, pp. 318–323, 2015.

[24] M. S. Liu, M. C. C. Lin, I. T. Huang, and C. C. Wang, "Enhancement of thermal conductivity with CuO for nanofluids," *Chemical Engineering & Technology*, vol. 29, no. 1, pp. 72–77, 2006.

[25] R. S. Vajjha and D. K. Das, "A review and analysis on influence of temperature and concentration of nanofluids on thermophysical properties, heat transfer and pumping power," *International Journal of Heat and Mass Transfer*, vol. 55, no. 15-16, pp. 4063–4078, 2012.

[26] S. R. Shamshirgaran, M. K. Assadi, H. H. al-Kayiem, and K. V. Sharma, "Investigation of thermal behaviour, pressure drop, and pumping power in a Cu nanofluid-filled solar flat-plate collector," *MATEC Web of Conferences*, vol. 131, article 01003, 2017.

[27] Z. Said, R. Saidur, N. A. Rahim, and M. A. Alim, "Analyses of exergy efficiency and pumping power for a conventional flat plate solar collector using SWCNTs based nanofluid," *Energy and Buildings*, vol. 78, pp. 1–9, 2014.

[28] V. Salamon, D. Senthil Kumar, and S. Thirumalini, "Experimental investigation of heat transfer characteristics of automobile radiator using tio2-nanofluid coolant," *IOP Conference Series: Materials Science and Engineering*, vol. 225, article 012101, 2017.

[29] H. F. Oztop and K. Al-Salem, "A review on entropy generation in natural and mixed convection heat transfer for energy systems," *Renewable and Sustainable Energy Reviews*, vol. 16, no. 1, pp. 911–920, 2012.